

# Vortex phase diagram of mesoscopic cylinder with suppressed surface superconductivity

W. V. Pogosov

*Moscow Institute of Physics and Technology,  
141700 Dolgoprudnyi, Moscow region, Russia*

Vortex structures in mesoscopic cylinder placed in external magnetic field are studied under the general de Gennes boundary condition for the order parameter. The Ginzburg-Landau equations are solved based on trial functions for the order parameter for vortex-free, single-vortex, multivortex, and giant vortex phases. The equilibrium phase diagrams and magnetization curves of mesoscopic cylinders are calculated at different values of de Gennes "extrapolation length" characterizing the boundary condition for the order parameter. The comparison of the obtained variational results with some known exact solutions shows good accuracy of our approach.

PACS numbers: 74.60.Ec, 74.24.Ha

## I. INTRODUCTION

Recent achievements in electronic device miniaturization allow one to study the mesoscopic superconducting samples with sizes of the order of the coherence length  $\xi(T)$ . Such structures attract a considerable current interest as a possible basis for low temperature electronics. The superconducting state was studied experimentally for different-shaped samples: discs, loops, double loops, dots etc. [1–4]. It was shown that the sample shape and sizes affect significantly the phase diagrams of the mesoscopic superconductors.

The vortex phases in mesoscopic superconductors are commonly studied within the framework of the Ginzburg-Landau theory [5–17]. The Ginzburg-Landau solutions for axially symmetric mesoscopic samples (cylinders, discs) can be subdivided into two different types [6–11]. In the first case the modulus of the local order parameter is axially symmetric inside the sample. The superconducting vortex-free state, the single-vortex state, and the giant-vortex state belong to this type of solutions. In the second case the axial symmetry is broken and a vortex cluster is formed inside the sample (multivortex phase). This state usually appears at lower fields and larger sample sizes as compared to the giant-vortex phase [7,8,10,11]. Note that multivortex state corresponds to the Abrikosov flux-line lattice for the bulk superconductors.

The vortex phases in mesoscopic superconductor can be characterized by "vorticity" that is the sum of angular quantum moments of all vortices and giant vortices.

With changing the applied magnetic field or temperature there are the first order phase transitions between the states with different vorticity or between different multivortex states with the same vorticity. The transitions between the multivortex and the giant vortex states with the same vorticity are of the second order [7–11].

The phase diagram of mesoscopic superconductor is strongly influenced by the boundary condition for the order parameter. In general case it is given by the de Gennes boundary condition [18,19]:

$$\mathbf{n}(-i\nabla - \mathbf{a})\psi = \frac{i}{b}\psi, \quad (1)$$

where  $\mathbf{n}$  is the unit vector normal to the sample surface,  $b$  is the de Gennes "extrapolation length",  $\mathbf{a}$  is the vector potential, and  $\psi$  is the order parameter. Here and below the following dimensionless variables are used: distances, magnetic field, and the order parameter are measured in units of coherence length  $\xi(T)$ , bulk upper critical field  $H_{c2}$ , and  $\sqrt{-\alpha/\beta}$ , respectively, with  $\alpha$ ,  $\beta$  being the Ginzburg-Landau coefficients. Microscopic considerations show that  $b \rightarrow \infty$  for the interface of conventional  $s$ -wave superconductor and vacuum [18–21], whereas  $b \sim 1$  ( $\xi(T)$  in dimensional units) for superconductor-normal metal,  $d$ -wave superconductor-vacuum, or anisotropic  $s$ -wave superconductor-vacuum interfaces [19–23]. It follows from Eq. (1) that the order parameter is suppressed in the vicinity of the sample surface at  $b \sim 1$ . There are also possibilities for the enhancement of the order parameter at the interface that can be described by negative  $b$  values. It can be realized by choosing the suitable material as a surrounding medium [24,25], i. e., a superconductor having a higher transition temperature than the material of the mesoscopic sample. Another possibility is to choose a semiconductor as a surrounding medium, such that there is a overlap of the band gap of the semiconductor with the superconducting gap. For the case of isotropic  $s$ -wave superconductor-vacuum interface ( $b \rightarrow \infty$ ), the magnetic properties of mesoscopic cylinders and discs, their equilibrium and non-equilibrium phase diagrams were studied in numerous papers, see e. g. Refs. [5–15], using different approaches. The vortex structures allowing for the enhanced surface superconductivity were studied in Refs. [24,25]. In Ref. [24] the case of mesoscopic discs was considered within the lowest Landau level approximation. In Ref. [25] the Ginzburg-Landau equations were solved numerically and self-consistently for superconducting state in long cylinders.

In this paper we study the vortex structures in mesoscopic cylinders under the general boundary condition for the order parameter corresponding to the *suppressed* surface superconductivity. For this purpose, we propose a variational approach and solve the Ginzburg-Landau equations without straightforward integration using trial functions for the order parameter. These trial functions are characterized by several variational parameters that allows one to describe the actual spatial distribution of the order parameter more accurately than in frequently used lowest Landau level approximation. The approach is applicable to all vortex phases (the vortex-free, the single-vortex, the multivortex, and the giant vortex states) and any values of de Gennes "extrapolation length". The comparison of variational calculations with some known exact results demonstrates good accuracy of our approximation. The model enables us to calculate the equilibrium phase diagram of the cylinder in the plane of the external field and the cylinder radius. The magnetization curves of the cylinder are calculated.

## II. MODEL

Let us consider a cylindrical type-II superconductor placed in the uniform external magnetic field parallel to the cylinder axis. The sample is assumed to be much longer than London penetration depth  $\lambda(T)$ . Therefore, both the order parameter and the magnetic field are constant along cylinder axis. We use the cylindrical coordinate system with coordinates  $r, \varphi, z$  and unit vectors  $\mathbf{e}_r, \mathbf{e}_\varphi, \mathbf{e}_z$ .

The system of Ginzburg-Landau equations is given by [26]:

$$|\psi|^2\psi - \psi + (i\nabla + \mathbf{a})^2\psi = 0, \quad (2)$$

$$\text{rot } \mathbf{h} = \frac{1}{\kappa^2} \left[ \mathbf{a}|\psi|^2 + \frac{i}{2} (\psi^* \nabla \psi - \psi \nabla \psi^*) \right], \quad (3)$$

where  $\mathbf{a}$ ,  $\mathbf{h}$ , and  $\psi$  are the dimensionless vector potential, local magnetic field, and the order parameter ( $\mathbf{h} = \text{rot } \mathbf{a}$ ,  $\mathbf{h} = h\mathbf{e}_z$ );  $\kappa$  is the Ginzburg-Landau parameter. Equations (2) and (3) must be supplemented by the boundary conditions for the order parameter (1) and the magnetic field:

$$h(R) = h_e, \quad (4)$$

where  $h_e$  is the external field. Next, we expand all variables in powers of  $\kappa$ :

$$\psi = \sum_{n=0}^{\infty} \psi_{2n} \frac{1}{\kappa^{2n}}, \quad \mathbf{a} = \sum_{n=0}^{\infty} \mathbf{a}_{2n} \frac{1}{\kappa^{2n}}, \quad h = \sum_{n=0}^{\infty} h_{2n} \frac{1}{\kappa^{2n}}. \quad (5)$$

We substitute expansions (5) to Ginzburg-Landau equations (2), (3) and to boundary conditions (1), (4)

and equate powers of  $\kappa$ . It is easy to show that the vector potential and the magnetic field at leading order are given by:

$$\mathbf{a}_0 = \mathbf{e}_\phi \frac{h_e r}{2}, \quad h_0 = h_e. \quad (6)$$

The order parameter at leading order  $\psi_0$  is determined by the first Ginzburg-Landau equation (2) and the boundary condition (1) at  $\mathbf{a} = \mathbf{a}_0$ . This condition is now given by:

$$\frac{\partial \psi_0}{\partial r} + \frac{\psi_0}{b} = 0. \quad (7)$$

In the next order one has from Eq. (3):

$$h_2 = - \int_0^r dr \mathbf{e}_\varphi \left[ |\psi_0|^2 \mathbf{a}_0 + \frac{i}{2} (\psi_0^* \nabla \psi_0 - \psi_0 \nabla \psi_0^*) \right]. \quad (8)$$

Thus, at leading order the magnetic field is uniform inside the sample and the magnetization equals zero. Physically, this implies that the additional field generated by the Meissner current and by the vortices is of the order of  $1/\kappa^2$  in comparison with the external uniform field. Below, we shall calculate the energy of the sample at leading order, whereas the magnetization will be found at the next order using Eq. (8). It was shown in Ref. [27] that this approximation is accurate not only for high- $\kappa$  materials but also for moderate- $\kappa$  superconductors (e.g.  $\kappa \approx 5$ ) with sizes comparable to  $\xi(T)$ .

We present  $\psi_0$  as a Fourier series:

$$\psi_0(r, \varphi) = \sum_{k=0}^{\infty} f_k(r) \exp(-ik\varphi). \quad (9)$$

For the axial symmetric distribution of the modulus of the order parameter inside the sample the only one term in Eq. (9) is nonzero. The vortex-free, single-vortex, and giant vortex phases with angular quantum momentum  $L$  correspond to the harmonics with  $k = 0, 1$ , and  $L$ , respectively. The modulus of the order parameter in the multivortex phase is not axially symmetric. Note that in this case the symmetry of the vortex configuration imposes a restriction on functions  $f_k$ : some of these functions equal zero. It was shown in Refs. [7,10] that taking into account only two main terms in right-hand side of Eq. (9) is enough for an accurate calculation of the energy of the mesoscopic superconductor in multivortex state. The vortex cluster with  $L$  vortices on a ring and no vortex at the axis (ring-like configuration) can be described as a mixture of two components with  $k_1 = 0$  and  $k_2 = L$ . The vortex cluster with one vortex at the cylinder axis and  $(L-1)$  vortices on a ring corresponds to  $k_1 = 1$  and  $k_2 = L$ . The contribution from other harmonics is small and can be neglected [7,10].

Using Eqs. (2) and (9) it can be easily shown that each function  $f_k(r)$  has the following asymptotic at  $r \rightarrow 0$ :

$$f_k(r) \sim r^k. \quad (10)$$

Besides, each function  $f_k(r)$  meets boundary condition (7). These conditions for  $f_k(r)$  are valid both for the giant vortex and the multivortex phases. It is a rather complicated task to find  $f_k(r)$  from the first Ginzburg-Landau equation (2) due to its non-linearity. Instead of the straightforward integration of the first Ginzburg-Landau equation, it is possible to use trial functions for the coordinate dependence  $f_k(r)$ . Notice that different variational procedures allowing one to solve approximately the Ginzburg-Landau equations were used in numerous papers for mesoscopic [7,10,15], bulk [28–31], and different-shaped [32] superconductors. We use here the following trial function for  $f_k(r)$  satisfying condition (10):

$$f_k(r) = p_1^k \exp \left( -q_k(p_2^k, p_3^k) \frac{r^2}{R^2} \right) \times \left( \left( \frac{r}{R} \right)^k + p_2^k \left( \frac{r}{R} \right)^{k+2} + p_3^k \left( \frac{r}{R} \right)^{k+4} \right), \quad (11)$$

where  $p_1^k, p_2^k, p_3^k$  are variational parameters, and the function  $q_k(p_2^k, p_3^k)$  is found from boundary condition (7):

$$q_k(p_2^k, p_3^k) = \frac{R}{2b} + \frac{k + p_2^k(k+2) + p_3^k(k+4)}{2(1 + p_2^k + p_3^k)}. \quad (12)$$

Trial function (11) was used in Ref. [32] for the study of surface superconductivity in samples of different complex shapes placed in vacuum ( $b \rightarrow \infty$ ).

The Ginzburg-Landau functional for the Gibbs free energy  $G$  of the cylinder can be written as a sum of two contributions,  $G_b$  and  $G_s$ . The former is the bulk energy of the sample and the latter is the surface energy. These contributions are given by [20,23,26]:

$$G_b = \int \left[ -|\psi|^2 + \frac{1}{2}|\psi|^4 + |(-i\nabla - \mathbf{a})\psi|^2 + \kappa^2 \mathbf{h}^2 - 2\kappa^2 \mathbf{h} \mathbf{h}_e \right] dV, \quad (13)$$

$$G_s = \frac{1}{b} \int |\psi|^2 dS. \quad (14)$$

The integration in Eqs. (13) and (14) is performed over the sample bulk and surface, respectively. Note that the general boundary condition for the order parameter (1) can be obtained by minimization of the free energy functional  $G = G_b + G_s$  with respect to the order parameter  $\psi$  and the vector potential  $\mathbf{a}$  [20,23,33].

Substituting expansion (9) to Eqs. (13) and (14) and taking into account Eq. (6) we obtain the expression for the energy of the multivortex state (per unit length of the cylinder):

$$G_b = 2\pi \int_0^R r dr \left[ \frac{1}{2} (f_{k_1}^4 + f_{k_2}^4 + 4f_{k_1}^2 f_{k_2}^2) - \right.$$

$$\left. f_{k_1}^2 - f_{k_1}^2 + \left( \frac{df_{k_1}}{dr} \right)^2 + \left( \frac{df_{k_2}}{dr} \right)^2 - \kappa^2 h_e^2 + f_{k_1}^2 \left( \frac{h_e r}{2} - \frac{k_1}{r} \right)^2 + f_{k_2}^2 \left( \frac{h_e r}{2} - \frac{k_2}{r} \right)^2 \right], \quad (15)$$

$$G_s = \frac{2\pi R}{b} (f_{k_1}^2(R) + f_{k_2}^2(R)). \quad (16)$$

For the case of the state with axially symmetric local order parameter one of functions  $f_{k_1}$  and  $f_{k_2}$  equals zero. Using Eqs. (11) and (12) we find the energy  $G$  from Eqs. (15) and (16) by a straightforward integration as an explicit function of variational parameters  $p_1^{k_1}, p_2^{k_1}, p_3^{k_1}$  and  $p_1^{k_2}, p_2^{k_2}, p_3^{k_2}$ . The resulting expression, however, is rather cumbersome and we do not present it here. Finally, the values of the variational parameters at each  $R$  are found numerically by the minimization of the free energy. This procedure yields the local order parameter and the energy of the cylinder. Notice that  $G$  is biquadratic with respect to the parameters  $p_1^{k_1}$  and  $p_1^{k_2}$  that simplifies appreciably the minimization procedure.

Knowing the local order parameter we can calculate the magnetization. It is given by:

$$-4\pi M = \langle h \rangle - h_e, \quad (17)$$

where  $\langle h \rangle$  is the averaged magnetic field over the superconductor volume. Taking into account Eq. (8) and expansion (9) we obtain:

$$-4\pi M = \frac{2}{\kappa^2 R^2} \int_0^R r dr \int_0^r dx \left[ f_{k_1}^2(x) \left( \frac{h_e x}{2} - \frac{k_1}{x} \right) + f_{k_2}^2(x) \left( \frac{h_e x}{2} - \frac{k_2}{x} \right) \right]. \quad (18)$$

Functions  $f_{k_1}$  and  $f_{k_2}$  are found by the method described above. Hence, one can calculate the magnetization using Eq. (18). In the following section we apply the developed approach for the analysis of the behavior of the cylinder in the external field.

### III. RESULTS AND DISCUSSION

Comparing the energies of different states one can calculate the equilibrium phase diagram of the cylinder. The results of our calculations are shown in Fig. 1 for different  $b$  values:  $b = 1$  (a),  $b = 2.5$  (b),  $b = 5$  (c), and  $b \rightarrow \infty$  (d). The latter case corresponds to the isotropic superconductor-vacuum interface, and was studied in Refs. [5,6,10,11,13–15]. Curve 1 shows the transition from the normal to the superconducting state (the surface critical field  $h_{c3}$ ). The oscillatory behavior of the function  $h_{c3}(R)$  is caused by the fact that the transition occurs from the normal to the giant vortex states

with different angular quantum moments  $L$  depending on the cylinder radius. Besides, the function  $h_{c3}(R)$  depends appreciably on the value of  $b$ : the value of  $h_{c3}(R)$  decreases with decrease of  $b$ . At  $R \rightarrow \infty$  the dependence  $h_{c3}(R)$  tends to the surface critical field for the half-space sample, which was calculated in Ref. [22] as a function of  $b$ . Note that  $h_{c3}(\infty) = 1.695$  for  $b \rightarrow \infty$  and  $h_{c3}(\infty) = 1$  for  $b \rightarrow 0$  [18,22].

Below  $h_{c3}$  the transitions between different giant vortex states take place. Solid lines show the phase boundaries between the states with different vorticity. In the giant vortex state the order parameter is strongly suppressed in the inner part of the cylinder, and this state can be referred to a surface superconductivity. For illustration, the spatial distribution of the order parameter in the giant vortex phase with  $L = 3$  is plotted in Fig. 2 at  $b = 1$ ,  $R = 4.625$ ,  $h_e = 0.75$  (a) and  $b \rightarrow \infty$ ,  $R = 3.6$ ,  $h_e = 1$  (b). In the former case the order parameter is also suppressed at the sample surface due to the small  $b$  value (superconductor -normal metal,  $d$ -wave superconductor-vacuum, or anisotropic  $s$ -wave superconductor-vacuum interfaces) [19,21,22].

As follows from Fig. 1, the superconducting state does not nucleate at very small cylinder radii, smaller than some critical radius, and the sample is in normal state at any applied field. The critical radius tends to zero at  $b \rightarrow \infty$ . There is also the interval of  $R$  for each  $b$ , when the vortex phase does not nucleate, and the transition occurs from the normal to the superconducting vortex-free state. Every vortex phase with vorticity  $L > 1$  can exist in the form of the giant vortex or the multivortex configuration. The dashed lines on Fig. 1 shows the boundaries between these states. Below these lines for given  $L > 1$  the multivortex state has the lowest energy, and above these curves the giant vortex state becomes more energetically favorable. In equilibrium state the multivortex phase can exist if the applied field is smaller than 1 ( $H_{c2}$  in dimensional units) and if the radius of the cylinder is large enough. For each  $b$  there exists an interval of small cylinder radii, when the multivortex phase is energetically unfavorable as compared to the states with axial symmetric distribution of the modulus of the order parameter. Curve 2 in Fig. 1 shows the lower critical field that corresponds to the equilibrium boundary between the vortex-free and the single-vortex states.

With increasing the external field the cylinder can follow rather complex set of phase transitions. It can come from the giant vortex to the multivortex states and then back to the giant vortex phase. For example, at  $R = 4.4$ ,  $b = 1$  the following set of transitions occurs:  $0 \rightarrow 1 \rightarrow 2_m \rightarrow 2_g \rightarrow 3_m \rightarrow 3_g \rightarrow 4_m \rightarrow 4_g$ , where the numbers denote the vorticity of the phase and indexes the type of the phase: "m" corresponds to the multivortex state, "g" to the giant vortex state. At  $R = 4.1$ ,  $b = \infty$  the set of transitions is:  $0 \rightarrow 1 \rightarrow 2_g \rightarrow 3_m \rightarrow 3_g \rightarrow 4_m \rightarrow 4_g \rightarrow 5_g \rightarrow 6_g \rightarrow 7_g \rightarrow 8_g \rightarrow 9_g \rightarrow 10_g \rightarrow 11_g$ .

The transition between the phases with different vorticity is always of the first order, it occurs when the en-

ergies of different states become equal. The transitions between the states with the same vorticity may be of the second as well as of the first order. The second order phase transitions occur between the multivortex and the giant vortex states. In this case, with increasing of the applied field the intervortex distances decrease, and vortices merge into the giant vortex located at the cylinder axis. Notice that the ring-like vortex clusters are energetically more favorable than the clusters with the vortex at the cylinder axis for the cylinder radii shown in Fig. 1. We found that for thicker cylinders at all  $b > 0$  the ground state is represented by configurations with the vortex at the sample axis. The transitions between multivortex states of the same vorticity with and without central vortex are of the first order.

Now we find the magnetization of the cylinder using Eq. (18). The results of our calculations at  $\kappa = 5$  are presented in Fig. 3(a) for  $b = 1$ ,  $R = 4.625$  and in Fig. 4(a) for  $b \rightarrow \infty$ ,  $R = 4.05$ . In these cases the cylinders are able to accommodate the giant vortices with maximum angular quantum moments equal to 5 and 11, respectively, before the transition to the normal state. Jumps in the magnetization correspond to the transitions between the states with different vorticity. In the first case at  $h_e \approx 0.61$  ( $0.61H_{c2}$  in dimensional units) the transition occurs from the multivortex state with 2 vortices to the giant vortex state with angular quantum momentum 2 ( $2_m \rightarrow 2_g$ ). In the second case the transition  $3_m \rightarrow 3_g$  occurs at  $h_e \approx 0.74$  and the transition  $4_m \rightarrow 4_g$  occurs at  $h_e \approx 0.87$ . All these transitions are followed by weak jumps in the slope of the magnetization. The behavior of the magnetization near the transitions is shown in Fig. 3(b) and 4(b). Solid lines denote the equilibrium magnetization, dashed lines denote the metastable magnetization corresponding to the giant vortex phase.

Next we discuss the accuracy of our variational procedure. First, we compare the variational results with known exact solutions for the surface critical field. The phases with axial symmetric distribution of the modulus of the order parameter are always energetically more favorable with respect to the multivortex state at applied field higher than the bulk upper critical field (see phase diagrams on Fig. 1). In the vicinity of the surface critical field the first Ginzburg-Landau equation (1) can be linearized. A resulting equation has the following analytical solution [5]:

$$f_L(R) = r^L \exp\left(-\frac{h_e r^2}{4}\right) \Phi\left(\frac{h_e - 1}{2h_e}, L + 1, \frac{h_e r^2}{2}\right), \quad (19)$$

where  $\Phi$  is Kummer function. Function (19) must meet the boundary condition (7). This yields the transcendental equation for the surface critical field allowing one to find  $h_{c3}(R)$  exactly. The comparison of the variationally calculated  $h_{c3}$  with this exact dependence shows good agreement with an accuracy better than 1% for all values of  $b$  and  $R$  under study. The lower critical field of the

cylinder  $h_{c1}$  versus  $R$  was calculated numerically in Ref. [12] at  $b \rightarrow \infty$ . The comparison of this result with our dependence  $h_{c1}(R)$  reveals the same accuracy. Thus, our results appear to be a good approximation to the exact Ginzburg-Landau solutions for the mesoscopic cylinders.

In summary, we analyzed the superconducting state in long mesoscopic cylinder with suppressed surface superconductivity. An asymptotic expansion was used to simplify the Ginzburg-Landau equations at high and moderate values of  $\kappa$ , and the simplified equations were solved by variational method. The equilibrium vortex phase diagrams of the cylinder were obtained in the plane of the cylinder radius and the applied field at different values of "extrapolation length". We showed that the phase diagram and magnetization depends appreciably on the value of "extrapolation length".

## ACKNOWLEDGMENTS

The author acknowledges useful discussions with K. I. Kugel, A. L. Rakhmanov, and E. A. Shapoval. This work was supported by the Russian Foundation for Basic Research (RFBR), grants Nos. 00-02-18032 and 01-02-06526, by the joint INTAS-RFBR program, grant No. IR-97-1394, and by the Russian State Program 'Fundamental Problems in Condensed Matter Physics'.

---

- [1] V. V. Moshchalkov, L. Gielen, C. Strunk, R. Jonckheere, X. Qiu, C. Van Haesendonck, and Y. Bruynseraede, *Nature* **373**, 319 (1995).
- [2] A. K. Geim, I. V. Grigorieva, S. V. Dubonos, J. G. S. Lok, J. C. Maan, A. E. Filippov, and F. M. Peeters, *Nature* **390**, 259 (1997).
- [3] A. K. Geim, S. V. Dubonos, I. V. Grigorieva, K. S. Novoselov, F. M. Peeters, and V. A. Schweigert, *Nature* **407**, 55 (2000).
- [4] V. Bruynndoncx, C. Strunk, and V. V. Moshchalkov, *Europhys. Lett.* **36**, 449 (1996).
- [5] V. V. Moshchalkov, X. G. Qiu, and V. Bruynndoncx, *Phys. Rev. B* **55**, 11793 (1997).
- [6] V. A. Schweigert and F. M. Peeters, *Phys. Rev. B* **57**, 13817 (1998).
- [7] V. A. Schweigert, F. M. Peeters, and P. S. Deo, *Phys. Rev. Lett.* **81**, 2783 (1998).
- [8] V. A. Schweigert and F. M. Peeters, *Phys. Rev. Lett.* **83**, 2409 (1999).
- [9] A. K. Geim, S. V. Dubonos, and J. J. Palacios, *Phys. Rev. Lett.* **85**, 1528 (2000).
- [10] J. J. Palacios, *Phys. Rev. B* **52**, R5948 (1998).
- [11] J. J. Palacios, *Phys. Rev. Lett.* **84**, 1796 (2000).
- [12] E. A. Shapoval, *Pis'ma Zh. Eksp. Teor. Fiz.* **69**, 532 (1999) [JETP Lett. **69**, 577 (1999)].

- [13] G. F. Zharkov, V. G. Zharkov, and A. Yu. Zvetkov, *Phys. Rev. B* **61**, 12293 (2000).
- [14] G. F. Zharkov, *Phys. Rev. B* **63**, 224513 (2001).
- [15] W. V. Pogosov, A. L. Rakhmanov, and E. A. Shapoval, *Physica C* **356**, 225 (2001).
- [16] V. R. Misko, V. M. Fomin, J. T. Devreese, and V. V. Moshchalkov, *Solid State Commun.* **114**, 499 (2000).
- [17] V. M. Fomin, J. T. Devreese, V. Bruyndoncx, and V. V. Moshchalkov, *Phys. Rev. B* **62**, 9186 (2000).
- [18] P. G. de Gennes, *Superconductivity of Metals and Alloys* (Addison-Wesley, New York, 1994).
- [19] P. G. de Gennes and J. Matricon, *Rev. Mod. Phys.* **36**, 45 (1964).
- [20] E. A. Andrushin, V. L. Ginzburg, and A. P. Silin, *Usp. Fiz. Nauk* **163**, 105 (1997) [Phys. Usp. **36**, 854 (1993)].
- [21] R. O. Zaitsev, *Zh. Eksp. Teor. Fiz.* **48**, 1759 (1965) [Sov. Phys. JETP **21**, 1178 (1965)].
- [22] E. A. Shapoval, *Pis'ma Zh. Eksp. Teor. Fiz.* **64**, 320 (1996) [JETP Letters **64**, 350 (1996)].
- [23] V. P. Mineev and K. V. Samokhin, *The Introduction to the Theory of Unconventional Superconductors*, Moscow, 1996 [in Russian].
- [24] S. V. Yampolskii and F. M. Peeters, *Phys. Rev. B* **62**, 9663 (2000).
- [25] B. J. Baelus, S. V. Yampolskii, F. M. Peeters, E. Montevercchi, and J. O. Indekeu, cond-mat/0106403 (2001).
- [26] D. Saint-James and G. Sarma, *Type II superconductivity*, Pergamon Press, 1969.
- [27] S. J. Chapman, Q. Du, M. D. Gunzburger, and J. S. Peterson, *Adv. Math. Sciences Appl.* **5**, 193 (1995).
- [28] H. Koppe and J. Willebrand, *J. Low Temp. Phys.* **2**, 499 (1970).
- [29] J. R. Clem, *J. Low Temp. Phys.* **18**, 427 (1975).
- [30] W. V. Pogosov, A. L. Rakhmanov, and K. I. Kugel, *Zh. Eksp. Teor. Fiz.* **118**, 676 (2000) [JETP **90**, 588 (2000)].
- [31] W. V. Pogosov, K. I. Kugel, A. L. Rakhmanov, and E. H. Brandt, *Phys. Rev. B* **64**, 064517 (2001).
- [32] R. C. Jones, M. K. Keene, and P. Nurwantoro, *Physica C* **298**, 140 (1998).
- [33] K. I. Kugel, W. V. Pogosov, and A. L. Rakhmanov, *Physica C* **339**, 10 (2000).

## FIGURE CAPTIONS

Fig.1. Equilibrium phase diagram of the cylinder in the external magnetic field at  $b = 1$  (a),  $b = 2.5$  (b),  $b = 5$  (c),  $b \rightarrow \infty$  (d). Solid lines show the boundaries between the states with different vorticity. Dashed lines correspond to the boundaries between the multivortex and the giant vortex phases. Curves 1 and 2 show the surface and the first critical fields, respectively. The dot line denotes the bulk upper critical field.

Fig 2. The spatial distribution of the dimensionless order parameter inside the mesoscopic cylinder in giant vortex state with angular quantum momentum  $L = 3$  at  $b = 1$ ,  $R = 4.625$ ,  $h_e = 0.75$  (a) and  $b \rightarrow \infty$ ,  $R = 3.6$ ,  $h_e = 1$  (b). The distance from the cylinder axis  $r$  is measured in units of the coherence length  $\xi(T)$ .

Fig. 3. The equilibrium magnetization of the cylinder with radius 4.625 versus applied field at  $b = 1$ ,  $\kappa = 5$ . Jumps in the magnetization in Fig. 3(a) correspond to the transitions between the states with different vorticity. Fig. 3(b) shows the behavior of the magnetization in the vicinity of the second order phase transition at  $H \approx 0.61H_{c2}$  from the multivortex state with 2 vortices to the giant vortex phase with vorticity  $L = 2$ . Solid lines correspond to the equilibrium magnetization, dashed line shows the magnetization of the metastable giant vortex phase.

Fig. 4. The equilibrium field dependence of the magnetization of the cylinder with radius 4.05 at  $b \rightarrow \infty$ ,  $\kappa = 5$ . In Fig. 4(b) the magnetization is plotted versus applied field near the transitions from the multivortex states to the giant vortex phases. Solid lines correspond to the equilibrium magnetization, dashed line shows the magnetization of the metastable giant vortex phase.

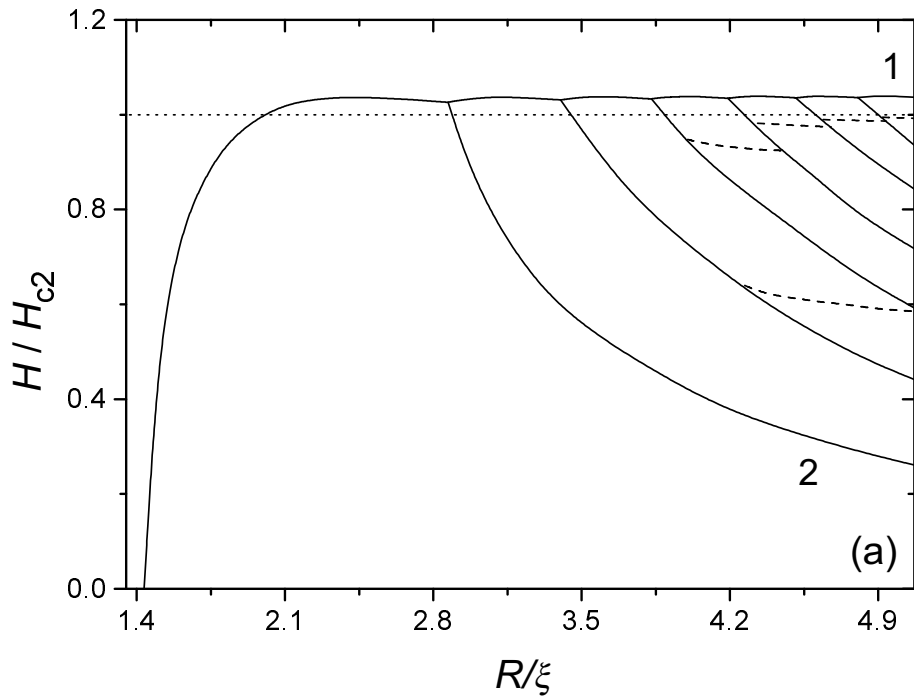


Fig. 1(a)

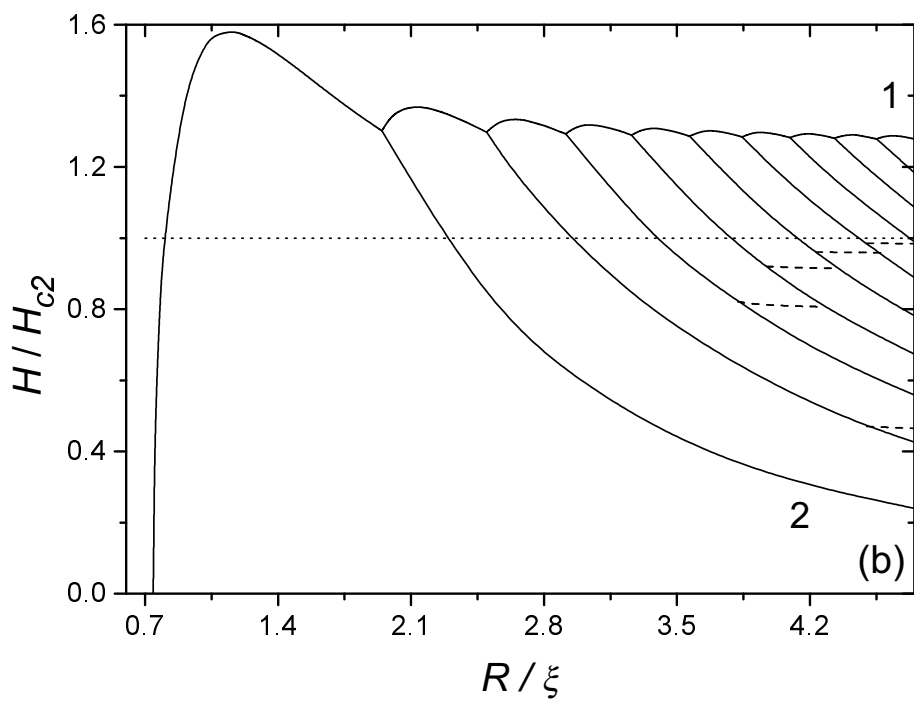


Fig. 1(b)

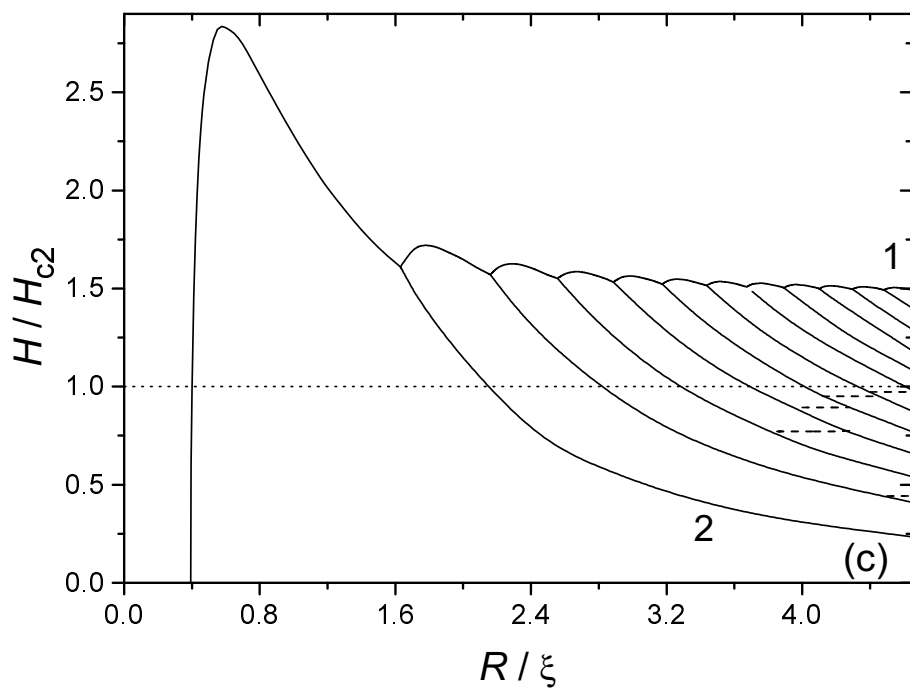


Fig. 1(c)

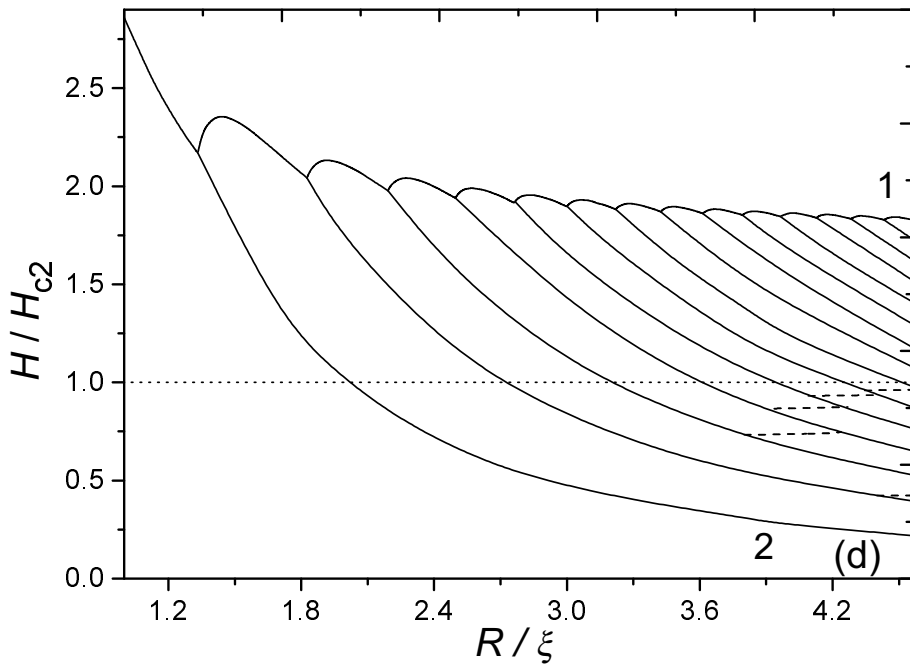


Fig. 1(d)

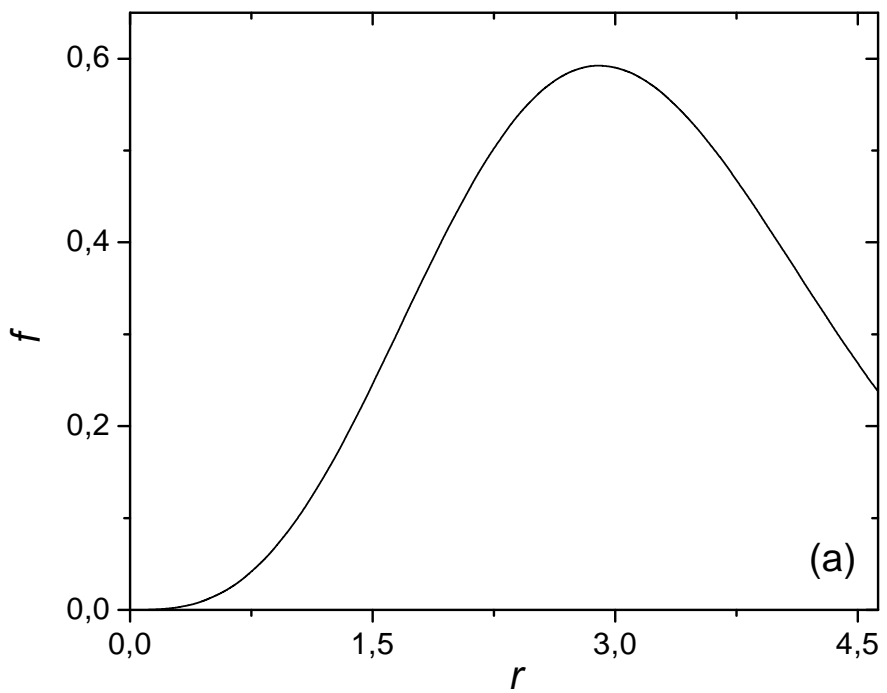


Fig. 2(a)

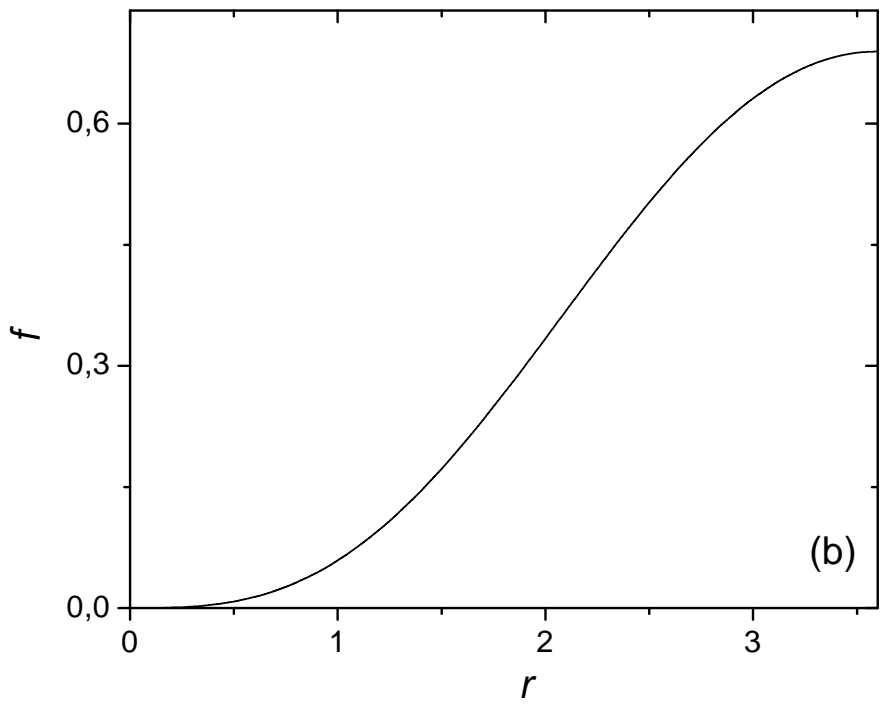


Fig. 2(b)

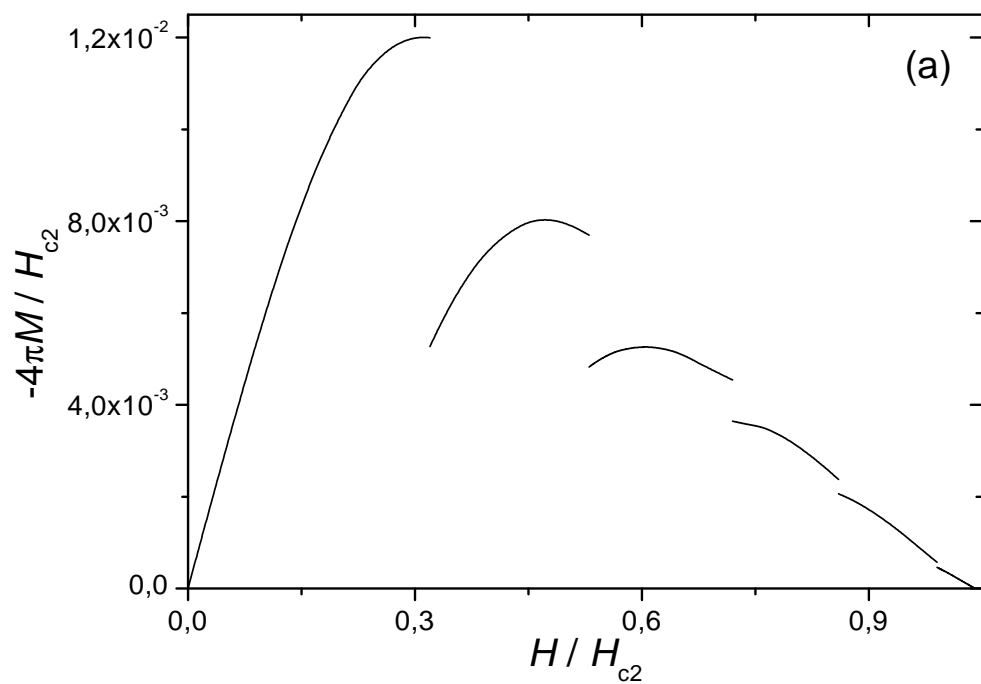


Fig. 3(a)

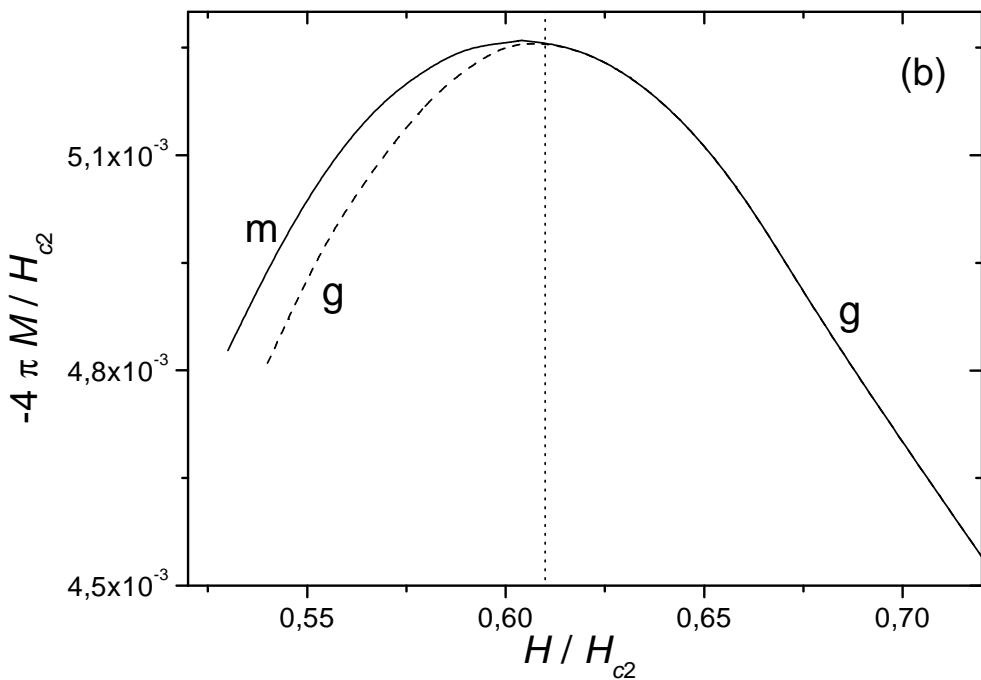


Fig. 3(b)

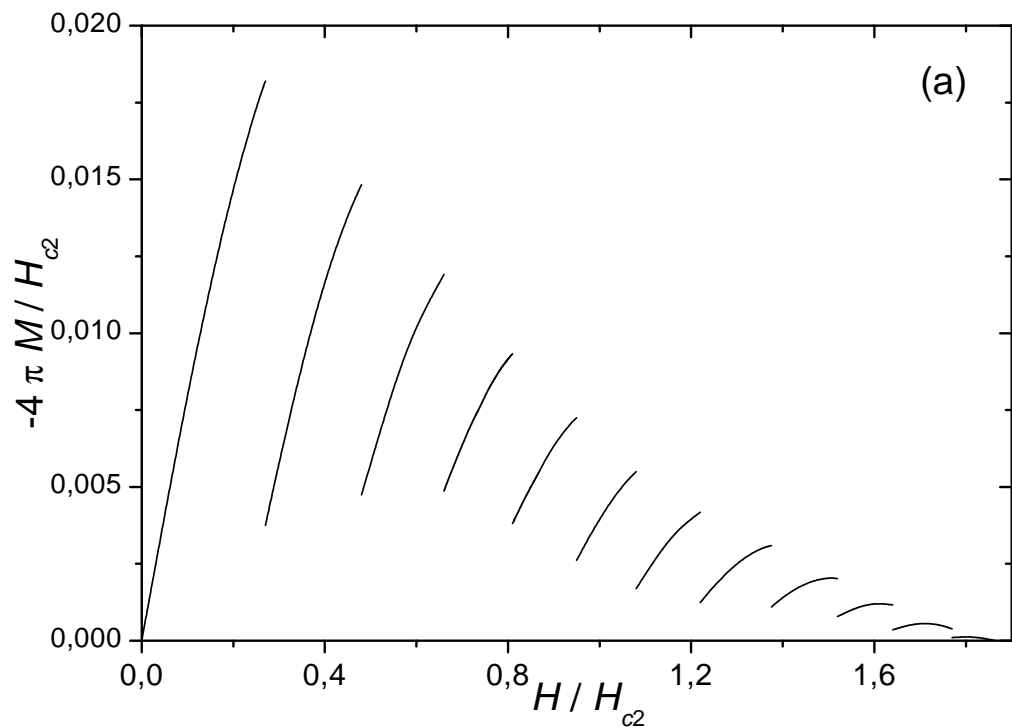


Fig. 4(a)

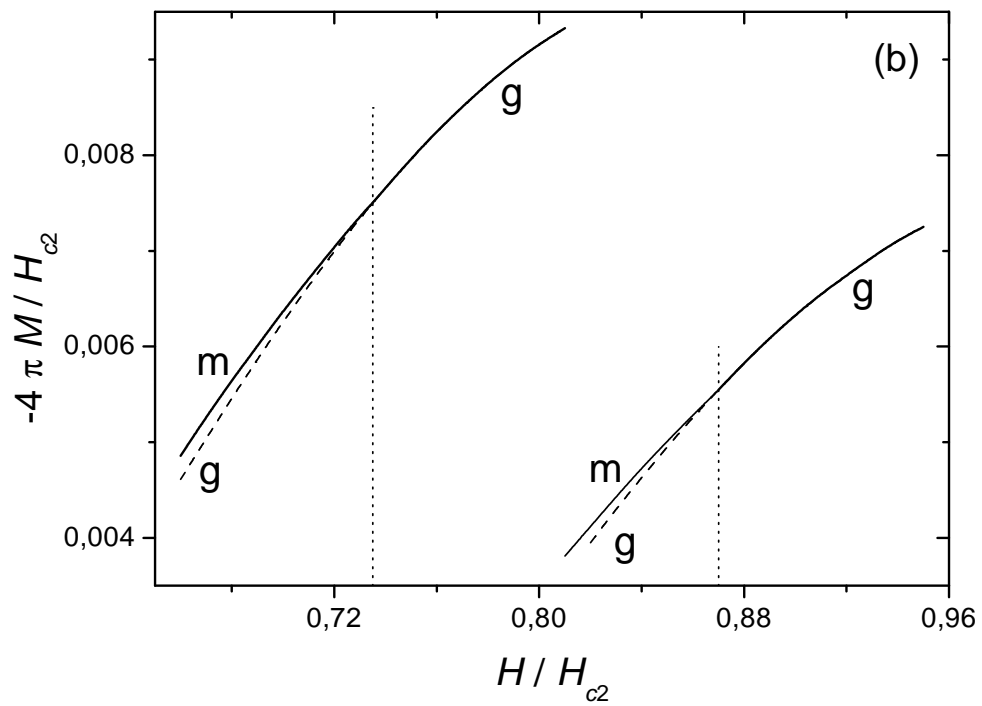


Fig. 4(b)